Available online at www.sciencedirect.com
SCIENCE DIRECT®
International Journal of Heat and Mass Transfer 48 (2005) 3615–3627
International Journal of HEAT and MASS TRANSFER
www.elsevier.com/locate/ijhmt

# Forced convective heat transfer across a pin fin micro heat sink

Yoav Peles *, Ali Koşar, Chandan Mishra, Chih-Jung Kuo, Brandon Schneider

*Department of Mechanical, Aerospace and Nuclear Engineering, Rensselaer Polytechnic Institute, Troy, NY 12180, USA*

Received 16 September 2004; received in revised form 2 March 2005
Available online 17 May 2005

**Abstract**

This paper investigates heat transfer and pressure drop phenomena over a bank of micro pin fins. A simplified expression for the total thermal resistance has been derived, discussed and experimentally validated. Geometrical and thermo-hydraulic parameters affecting the total thermal resistance have been discussed. It has been found that very low thermal resistances are achievable using a pin fin heat sink. The thermal resistance values are comparable with the data obtained in microchannel convective flows. In many cases, the increase in the flow temperature results in a convection thermal resistance, which is considerably smaller than the total thermal resistance.


*Keywords:* Microscale; Heat sink; Pin fins; Cross flow; MEMS; Microchannels

## 1. Introduction

Over the last decade, driven by the rapidly increasing heat dissipation predicament involving microprocessors, numerous investigations have been conducted on forced convection in microchannels concerning both single-phase [1–4] and boiling (two-phase flow) [5–9]. Nonetheless, other microscale cooling methods have received inadequate attention. This is perhaps because channels are fundamental geometries in heat transfer and fluid flow engineering applications, and extensive literature and knowledge exist for conventional scale channels. Furthermore, the relative ease of fabricating microchannels has ensured their popularity among researchers. However, recent advances in microfabrication technology have enabled the realization of alternate microscale cooling methods, whose performance can outshine the standards set by microchannels. At the conventional scale, pin fin heat sinks, either shrouded or open ended, are widely used in the industry. Nevertheless, very limited studies of such cooling methods have been conducted at the microscale.

Over the past century, several investigators have explored various heat transfer and pressure drop characteristics for flow across a bank of tubes at the macro scale and a considerable amount of data and correlations for heat transfer coefficients (Nusselt number) and friction factors are readily available in the literature. Explicit correlations for various flow regimes (laminar, transitional, or turbulent), pin fin arrangements (staggered or in-line) and pin geometry including longitudinal/transverse pitch-to-diameter ratio and pin height-to-diameter ratio ($L/D$) have been developed. Since cross flow over a long array of tubes is commonly encountered in shell-and-tube heat exchangers, early studies have mainly focused on arrays of long cylinders with $L/D > 8$ [10,11]. An assortment of correlations for different array configurations and flow regimes are readily available. Dimensional

* Corresponding author. Tel.: +1 518 276 2886; fax: +1 518 276 2623.
*E-mail address:* pelesy@rpi.edu (Y. Peles).

0017-9310/$ - see front matter © 2005 Elsevier Ltd. All rights reserved.
doi:10.1016/j.ijheatmasstransfer.2005.03.017

**Nomenclature**

| | |
|---|---|
| $A_b$ | base area [$m^2$] |
| $A_c$ | frontal cross-sectional area [$m^2$] |
| $A_{fc}$ | fin cross-sectional area [$m^2$] |
| $A_{fin}$ | fin surface area [$m^2$] |
| $A_{nf}$ | area defined in Eq. (7) |
| $A_p$ | platform area [$m^2$] |
| $A_t$ | total effective heat transfer area [$m^2$] |
| $C, C_2, C_3$ | constants |
| $c_p$ | specific heat at constant pressure [kJ $kg^{-1}$ °$C^{-1}$] |
| $D$ | pin fin hydraulic diameter [m] |
| $E$ | voltage applied across the heater [V] |
| $f$ | friction factor |
| $\bar{h}$ | average heat transfer coefficient [W $m^{-2}$ °$C^{-1}$] |
| $I$ | current passed through the device [A] |
| $k_{fin}$ | thermal conductivity of the fin [W $m^{-1}$ °$C^{-1}$] |
| $k_{fluid}$ | thermal conductivity of the fluid [W $m^{-1}$ °$C^{-1}$] |
| $L$ | channel height, fin height [m] |
| $m$ | constant |
| $\dot{m}$ | mass flowrate [kg $s^{-1}$] |
| $M$ | number of data points |
| MAE | mean absolute error |
| $n$ | constant |
| $N_{row}$ | number of pin fins in a single row |
| $N$ | number of pin fins in a single column |
| $\overline{Nu}$ | average Nusselt number |
| $P$ | electrical power [W], pressure |
| $\Delta P$ | pressure drop [kPa] |
| $P_f$ | fin perimeter [m] |
| $Pr$ | Prandtl number |
| $q''$ | heat flux [W $cm^{-2}$] |
| $Q$ | volumetric flowrate [$m^3$ $s^{-1}$] |
| $R$ | electrical resistance [Ω] |
| $R_{conv}$ | thermal resistance due to conduction [K $W^{-1}$] |
| $Re$ | Reynolds number based on pin fin hydraulic diameter |
| $R_{heat}$ | thermal resistance due to the increase in liquid temperature [K $W^{-1}$] |
| $R_{conv}$ | thermal resistance due to convection [K $W^{-1}$] |
| $R_{tot}$ | total thermal resistance [K $W^{-1}$] |
| $\overline{R}_{tot}$ | dimensionless total thermal resistance |
| $t$ | thickness of the silicon block [m] |
| $t_w$ | endwalls thickness [m] |
| $T$ | temperature [°C] |
| $V$ | frontal velocity [m $s^{-1}$] |
| $w_1$ | channel width [m] |
| $w_2$ | channel length [m] |
| $X$ | parameter under investigation |

*Greek symbols*

| | |
|---|---|
| $\Delta T_{av}$ | temperature difference between $T_{av}$ and $T_{amb}$ [°C] |
| $\varepsilon$ | porosity |
| $\eta$ | fin efficiency |
| $\mu$ | viscosity [kg $m^{-1}$ $s^{-1}$] |
| $\pi_1$ | second term of the right hand side in Eq. (13) |
| $\rho$ | density [kg $m^{-3}$] |

*Subscripts*

| | |
|---|---|
| amb | ambient |
| av | average |
| exp | experimental |
| in | inlet |
| min | minimum |
| s | surface |
| th | theoretical |
| exit | exit |

analysis suggests that the convective heat transfer across cylinders in cross flows varies with the Reynolds and Prandtl numbers. A commonly used relation for the average Nusselt number is in the following form $\overline{Nu} = CRe_D^m Pr^n$, where $C$, $m$, $n$ are constants. Various constants for different tube configurations and thermo-hydraulic conditions have been proposed, and it has been experimentally determined that the exponent $n$ lies between 0.3 and 0.4 [11]. Pressure drops have been expressed in terms of the velocity, number of rows, fluid density, and the friction factor. Besides, various correlations have been proposed for the friction factor for flow across a bank of tubes (e.g., [12]).

The knowledge gained through studies involving long tubes has contributed immensely to the development of various pin fin heat sinks. As noted by Moores and Joshi [13], intermediate size shrouded pin fin ($1/2 < L/D < 8$) heat sinks are primarily encountered in applications concerning turbine blade or vane cooling, whereas short pins are commonly found in compact heat exchangers [14]. A concise review of staggered array arrangements for intermediate pin sizes is provided by Armstrong and Winstanley [15]. In general, the average heat transfer coefficient for relatively short pin fins is slightly lower than for long cylinders. Friction factors, on the other hand, display no such deviation. However, Short et al. [16] have found that at low Reynolds numbers friction factors are altered for intermediate size tubes. This has an important implication for microscale pin fin heat sinks, since laminar flow is expected to dominate in these

systems. As a result, Koşar et al. [17] experimentally obtained friction factors over intermediate size 50 μm and 100 μm pin fin heat sink and demonstrated the importance of fin height-to-diameter ratio. Recently, Marques and Kelly [18] experimentally studied a heat exchanger possessing 500 μm diameter staggered micro pin fins with a pitch-to-diameter ratio of 2.5, which they fabricated using a modified LIGA (Lithography, Electroforming (German: Galvanoformung), and molding (German: Abformung)) micromachining process. An increase from 4.1 to 5.5 in the heat transfer rate has been reported with the introduction of pin fins for Reynolds number ranging from 4000 to 20 000.

The extensive knowledge of convective flow across a bank of pin fins presents an indispensable engineering tool that can be used to correlate the thermo-hydraulic field in such flow configurations. Although, it was developed mainly in the context of conventional scale systems it provides an excellent platform for extension to microscale devices, and can be employed to obtain preliminary heat transfer and pressure drop data. Due to the small pin dimensions at the microscale, the flow regime is expected to be predominantly laminar. Moreover, as stated by Incropera and DeWitt [19], a staggered fin arrangement is favored for enhanced heat transfer rates at low Reynolds numbers. The present study introduces the microscale pin fin heat sink design and concept, and analyzes its heat transfer capabilities. A test case that demonstrates the thermo-hydraulic performance of the micro heat sink is discussed in Section 3. In Section 4, preliminary experimental results, which support the analytical work, have been presented.

## 2. Microscale pin fin heat sink concept and heat transfer analysis

The concept of microchannel cooling integrated as part of the silicon substrate has been extensively investigated over the past decade. Relatively, insufficient attention has been given to other silicon based microscale cooling methods. A particular concept that will be examined in this study is presented in Fig. 1. A silicon heat sink is configured from a bank of pin fins, which are confined between endwalls. Liquid (or gas) flows across the array of pins and absorbs the heat generated by the heater at the base. As in microchannel heat sinks, the primary objective is to minimize the base temperature while maintaining pressure drops (or pumping power) as low as possible. A very useful performance parameter for the pin fin heat sink concept (as well as for other configurations) is the thermal resistance between the base and the cooling fluid.

The total thermal resistance ($R_{tot}$) can be expressed (similar to Tuckerman and Pease [20] and the analysis presented by Phillips in [21]) as the sum of three components that account for conduction through the silicon substrate excluding the fin region ($R_{cond}$), convection to the flow ($R_{conv}$), and thermal resistance due to an increase in the flow temperature as it flows through the fins and absorbs heat ($R_{heat}$). Since the substrate thickness is usually small (<500 μm) and the thermal conductivity of silicon is large (~150 W m$^{-1}$ °C), $R_{cond}$ is usually very small and for most practical purposes can be neglected. Using a simple energy balance $R_{heat}$ can be expressed as:

$$R_{heat} = \frac{1}{\dot{m}c_p} \tag{1}$$

Similarly, $R_{conv}$ can be expressed as:

$$R_{conv} = \frac{1}{\bar{h}A_t} \tag{2}$$

where $A_t$ is the total effective heat transfer area, which can be expressed as follows:

$$A_t = A_b + \eta A_{fin} \tag{3}$$

where $A_b$ is the base area, $A_{fin}$ the surface area of the fins, and $\eta$ the fin efficiency. From Eqs. (1)–(3) it follows:

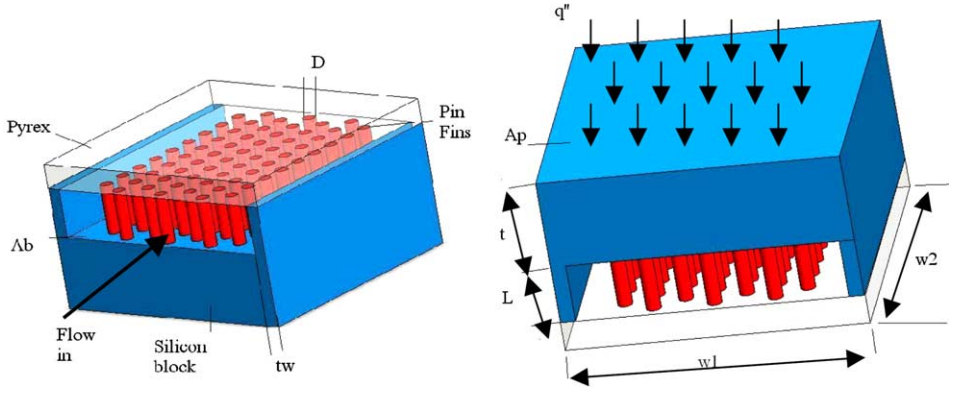


Fig. 1. Micro pin fin heat sink concept.

$$R_{\mathrm{tot}} = \frac{1}{\dot{m}c_p} + \frac{1}{\bar{h}(A_{\mathrm{b}} + \eta A_{\mathrm{fin}})} \tag{4}$$

Eq. (4) is multiplied by $\dot{m}c_p$ to obtain the dimensionless form of the thermal resistance:

$$\overline{R}_{\mathrm{tot}} = R_{\mathrm{tot}}\dot{m}c_p = 1 + \frac{\rho V A_{\mathrm{c}} c_p}{\bar{h}A_{\mathrm{b}}[1 + 4(1-\varepsilon/\varepsilon)\eta L/D]} \tag{5}$$

where $D$ is the pin fin hydraulic diameter, which is given by $4A_{\mathrm{fc}}/P_{\mathrm{f}}$, and $\varepsilon$ the porosity given by:

$$\varepsilon = \frac{A_{\mathrm{b}}}{A_{\mathrm{nf}}} \tag{6}$$

$A_{\mathrm{nf}}$ is related to the platform area of the heat sink (see Fig. 1), $A_{\mathrm{p}}$, by:

$$A_{\mathrm{nf}} = A_{\mathrm{p}} - 2t_{\mathrm{w}}W_2 \tag{7}$$

For an insulated fin tip, the fin efficiency is given as:

$$\eta = \frac{\tanh\left(2L\sqrt{\bar{h}/k_{\mathrm{fin}}D}\right)}{\left(2L\sqrt{\bar{h}/k_{\mathrm{fin}}D}\right)} \tag{8}$$

The ratio $A_{\mathrm{b}}/A_{\mathrm{c}}$ can be expressed as follows:

$$\frac{A_{\mathrm{b}}}{A_{\mathrm{c}}} = \frac{w_2}{L}C_2 \tag{9}$$

where $C_2$ is a geometrical constant. For evenly distributed circular fins on a square base area:

$$C_2 = \varepsilon/(1 - \sqrt{4(1-\varepsilon)/\pi}) \tag{10}$$

Note that for circular fins $(1 - \pi/4) < \varepsilon < 1$. Inserting Eqs. (8) and (9) into Eq. (5) yield:

$$\overline{R}_{\mathrm{tot}} = 1 + \frac{\rho V c_p}{\bar{h}\left(\frac{w_2}{L}\right)C_2\left[1 + \left(4\frac{1-\varepsilon}{\varepsilon}\right)\left(\frac{L}{D}\right)\frac{\tanh\left(2L\sqrt{\bar{h}/k_{\mathrm{fin}}D}\right)}{\left(2L\sqrt{\bar{h}/k_{\mathrm{fin}}D}\right)}\right]} \tag{11}$$

After some manipulations, it follows:

$$\overline{R}_{\mathrm{tot}} = 1 + \frac{Re\cdot Pr}{\overline{Nu}\left(\frac{w_2}{L}\right)C_2\left\{1 + 2\left(\frac{1-\varepsilon}{\varepsilon}\right)\frac{\tanh[2(L/D)\sqrt{\overline{Nu}\cdot k_{\mathrm{fluid}}/k_{\mathrm{fin}}}]}{\sqrt{\overline{Nu}\cdot k_{\mathrm{fluid}}/k_{\mathrm{fin}}}}\right\}} \tag{12}$$

The Nusselt number can be expressed in terms of the Reynolds and Prandtl numbers by [10]:

$$\overline{Nu} = C_3 Re^m Pr^{0.36}\left(\frac{Pr}{Pr_{\mathrm{s}}}\right)^{0.25} \tag{13}$$

From Eqs. (12) and (13) it can be seen that the total thermal resistance is a function of geometrical ($L/D$, $\varepsilon$, $W_2/L$) and thermo-hydraulic parameters ($Re_D$, $Pr$, $k_{\mathrm{fluid}}/k_{\mathrm{fin}}$). Eqs. (12) and (13) can be further simplified to obtain an expression for $\overline{R}_{\mathrm{tot}}$ in terms of a single dimensionless convection parameter ($\pi_1$):

$$\overline{R}_{\mathrm{tot}} = 1 + \pi_1 \tag{14}$$

where

$$\pi_1 = \frac{Re^{1-m}Pr^{0.64}}{C_3C_2\left(\frac{w_2}{L}\right)\left(\frac{Pr}{Pr_{\mathrm{s}}}\right)^{0.25}\left\{1 + 2\left(\frac{1-\varepsilon}{\varepsilon}\right)\frac{\tanh\left[2(L/D)\sqrt{C_3Re^mPr^{0.36}(Pr/Pr_{\mathrm{s}})^{0.25}k_{\mathrm{fluid}}/k_{\mathrm{fin}}}\right]}{\sqrt{C_3Re^mPr^{0.36}(Pr/Pr_{\mathrm{s}})^{0.25}k_{\mathrm{fluid}}/k_{\mathrm{fin}}}}\right\}} \tag{15}$$

Eqs. (14) and (15) clearly demonstrate the dependency of the thermal resistance on the geometrical configuration, the Reynolds ($Re$) and the Prandtl ($Pr$) numbers (not the heat flux). It follows that for a given pin fin configuration, $Re$ and $Pr$ number, the thermal resistance is constant for any heat flux. Thermal resistance obtained under a certain heat flux can be used without any modification to find the surface temperature for a different $q''$ (provided the geometrical configuration, $Re$ and $Pr$ numbers are not altered).

In Eq. (14), the first term on the right hand side (the unit value) accounts for the thermal resistance due to the increase in fluid temperature, while $\pi_1$ accounts for the convection thermal resistance. It follows from Eq. (14), that low values of the total thermal resistance can be achieved if $\pi_1$ is kept as low as possible. For $\pi_1 \ll 1$ convection is practically negligible and the temperature rise of the walls are only due to an increase of the fluid temperature. For $\pi_1 \gg 1$ convection is the dominant factor causing the wall temperature to rise. It would therefore be useful to assess the values of $\pi_1$, which correspond to typical conditions observed in electronic chip cooling. A typical micro scale pin fin heat sink is expected to have the following geometrical configurations and will operate in thermal-fluid conditions given by: $10 < Re < 1000$, $2 < L/D < 20$ ($200\ \mu\mathrm{m} < L < 400\ \mu\mathrm{m}$, $20\ \mu\mathrm{m} < D < 100\ \mu\mathrm{m}$), $20 < w_2/L < 200$ ($w_2 \sim 1$ cm), $0.5 < \varepsilon < 0.9$ (corresponding to circular pins with a pitch to diameter ratio of 1.25 and 3, respectively), and $C_3 \sim 0.9$, $m \sim 0.4$. It follows that $\pi_1$ has the following range:

$$0.0013 < \pi_1 < 4.2 \quad \text{for water} \tag{16}$$

$$0.0001 < \pi_1 < 1.2 \quad \text{for air} \tag{17}$$

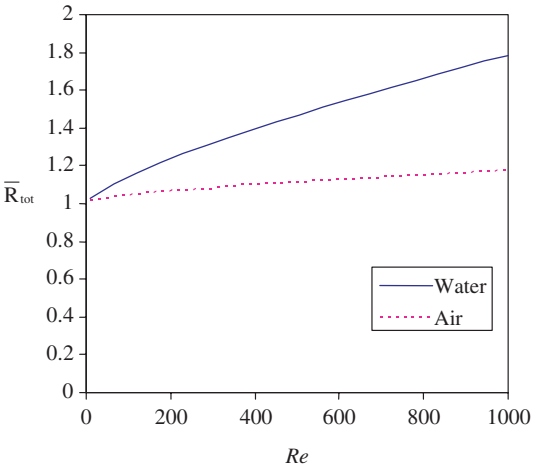


Fig. 2. $\overline{R}_{tot}$ vs. $Re$ evenly distributed pin fins with $\varepsilon = 0.65$, $C_2 = 1.953$, $C_3 = 0.9$, and $w_2/L = 25$.

The extremely low values of $\pi_1$ are indeed very encouraging. However, the higher values of $\pi_1$ suggest that careful consideration should be given to minimizing convection heat transfer in the heat sink design process.

Eq. (14) with $\pi_1$ from Eq. (15) is plotted in Fig. 2 for evenly distributed pin fins with $\varepsilon = 0.65$, $C_2 = 1.953$, $C_3 = 0.9$, and $w_2/L = 25$. As can be seen, $\overline{R}_{tot}$ tends to increase with the Reynolds number. This is because the power dependency of the Nusselt number on the Reynolds number is smaller than unity ($Re_D^m$) while the mass flow rate dependency is linear. The combined effect results in the $Re_D^{1-m}$ term in the numerator of $\pi_1$. The convective resistance is further increased by the reduction of the fin efficiencies at higher Nusselt numbers (higher Reynolds numbers). Fig. 2 also shows that $\overline{R}_{tot}$ of air is considerably lower than water. Besides, the density and thermal capacity of air is much lower than the corresponding values of water (3 orders of magnitude and 4 times lower, respectively). Therefore, the dimensional total resistance is considerably high for any practical engineering purpose.

The total thermal resistance as a function of the porosity for various Reynolds numbers (10, 100 and 1000) is shown in Fig. 3. As expected, low pin density (higher porosity) results in higher $\overline{R}_{tot}$. At low porosity ($\varepsilon$ smaller than ~0.7), the thermal resistance is primarily due to an increase in the fluid temperature as it flows through the heat sink and absorbs heat. At these $\varepsilon$ values the increase in $\overline{R}_{tot}$ is relatively minute, but for higher porosity $\overline{R}_{tot}$ increases steeply. To suppress the convective thermal resistance at high Reynolds number, dense pin fin configurations are preferable, while for low Reynolds numbers more sparse arrangements are sufficient. It should be noted that at very high porosity values the ratio $A_{fin}/A_b$ is small and Eq. (15) is no longer valid, since endwall effects dominate heat transfer. For $\varepsilon = 1$

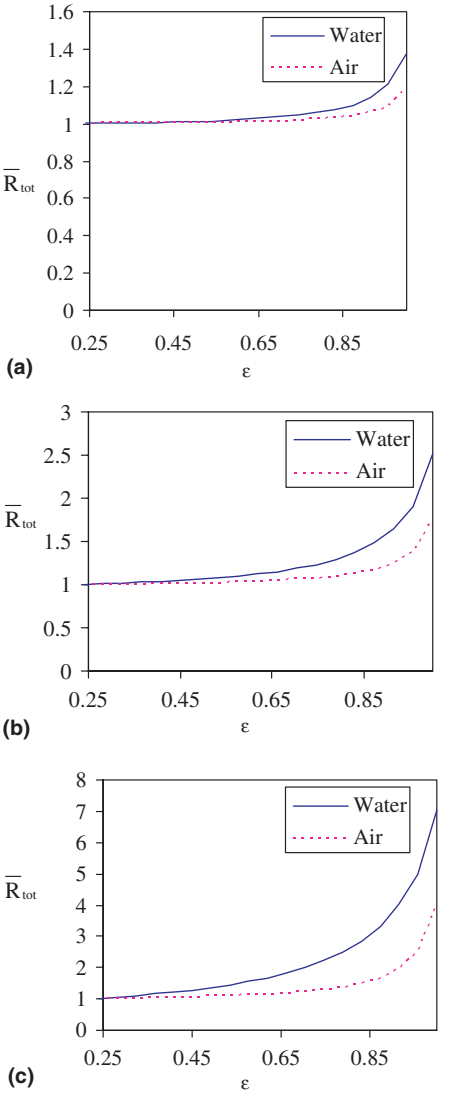


Fig. 3. $\overline{R}_{tot}$ vs. $\varepsilon$ profile for (a) $Re = 10$, (b) $Re = 100$, and (c) $Re = 1000$.

and high Reynolds numbers, the thermal resistance is considerably larger than the value given in Fig. 3 since the Nusselt number for channels (the microchannel between the endwalls) is a constant ($Nu \sim 5$ for large aspect ratio channels). However, for cylinders in cross flow $Nu$ increases with $Re$.

### 2.1. Pressure drop

Several optimization schemes for electronic cooling heat sinks have been previously examined [20,22–27]. All previous microscale cooling studies have employed the thermal resistance as the parameter to be minimized while maintaining a fixed pressure drop [22–25,27] or

pumping power [26] except for Murakami and Mikić [27] who minimized the pressure drop and pumping power for a fixed thermal resistance. Therefore, to initiate a valid comparison of the pin fin heat sink performance to other microchannel cooling schemes, it is useful to explicitly express the thermal resistance in terms of the pressure drop. The pressure drop, $\Delta P$, across a tube bank is given by Zukauskas [10]:

$$\Delta P = N\rho\frac{V^2}{2}f \tag{18}$$

where the friction factor, $f$, is given by [28] (for laminar flow and evenly distributed pin fins):

$$f = \frac{180}{Re}\left(\frac{\varepsilon}{1-\varepsilon}\right)^{0.4} \tag{19}$$

Inserting Eq. (19) into Eq. (18) and rearranging yields:

$$Re = \frac{\rho D^2}{90\mu^2 N}\left(\frac{1-\varepsilon}{\varepsilon}\right)^{0.4}\Delta P \tag{20}$$

Inserting Eq. (20) into Eq. (15) results in a direct relation between $\pi_1$ and the pressure drop:

$$\pi_1 = \frac{\left[\frac{\rho D^2}{90\mu^2 N}\left(\frac{1-\varepsilon}{\varepsilon}\right)^{0.4}\Delta P\right]^{1-m} Pr^{0.64}}{C_3 C_2\left(\frac{w_2}{L}\right)\left(\frac{Pr}{Pr_s}\right)^{0.25}\left\{1+2\left(\frac{1-\varepsilon}{\varepsilon}\right)\frac{\tanh\left[2(L/D)\sqrt{C_3\left(\frac{\rho D^2}{90\mu^2 N}\left(\frac{1-\varepsilon}{\varepsilon}\right)^{0.4}\Delta P\right)^m Pr^{0.36}(Pr/Pr_s)^{0.25}k_{fluid}/k_{fin}}\right]}{\sqrt{C_3\left(\frac{\rho D^2}{90\mu^2 N}\left(\frac{1-\varepsilon}{\varepsilon}\right)^{0.4}\Delta P\right)^m Pr^{0.36}(Pr/Pr_s)^{0.25}k_{fluid}/k_{fin}}}\right\}} \tag{21}$$

In order to fully define $\overline{R}_{tot}$ in terms of the pressure drop, the mass flow rate has to be correlated with respect to the pressure drop. After some manipulations the mass flow rate can be expressed as follows:

$$\dot{m} = \left[\frac{\rho D^3}{90\mu}\left(\frac{N_{row}}{N}\right)\left(\frac{L}{D}\right)\left(\frac{1-\varepsilon}{\varepsilon}\right)^{0.4}\left(\sqrt{\frac{\pi}{4(1-\varepsilon)}}-1\right)\right]\Delta P \tag{22}$$

The aforementioned analysis will now be demonstrated through a test case tailored to chip cooling application.

## 3. Test case: silicon heat sink for chip cooling

A typical silicon micro heat sink has a base area of 1 cm × 1 cm, substrate thickness of ~500 μm, which results in a maximum fin height of ~400 μm. A staggered array of circular fins is selected as the heat sink geometrical configuration, and water as the working liquid. Initially a pin fin pitch-to-diameter ratio of 1.5 is selected, which corresponds to $\varepsilon = 0.651$, $w_2/L = 25$, and $C_2 = 1.953$.

Total dimensional thermal resistance can be found for a given pressure drop by inserting Eqs. (21) and (22) into Eq. (14). $R_{tot}$ as a function of tube diameter for various pressure drops is shown in Fig. 4 for $L = 400$ μm (note that flow rate varies with the pin fin diameter for a given pressure drop). At small diameters (below ~50 m), $R_{tot}$ rapidly decreases as the diameter increases. As the fin diameter is further increased the curve slope gradually diminishes, and at some point a minimum is reached. Additional increase in the fin diameter results in higher thermal resistance. This is a result of two competing factors that affect $R_{tot}$ as $D$ is varied. On one hand, the heat transfer coefficient is inversely proportional to the fin diameter for a given Reynolds number. On the other hand, smaller diameters result in lower Reynolds numbers for a given mass flow rate, and higher friction factors, which elevates flow resistance. Therefore, for a fixed pressure drop, flow rates are reduced, which in turn reduces the heat transfer coefficient. At very small diameters (below ~50 μm) flow

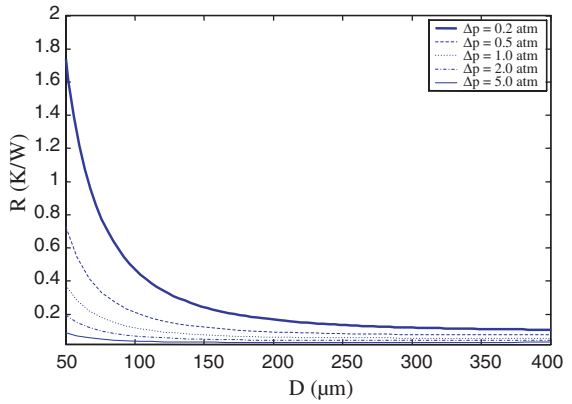


Fig. 4. $R_{tot}$ vs. $D$ for water ($L = 400$ μm, $\varepsilon = 0.65$, $w_2/L = 25$).

resistance dominates the high values of $R_{tot}$, while at large diameters $R_{tot}$ is dominated by the reduction in the heat transfer coefficient as the diameter increases.

The values of $D$, which minimize the thermal resistance, are shown in Fig. 5 to be between 250 and 325 μm at various values of the pressure drop. As the pressure drop decreases, the minimum shifts to a higher value. Higher pressure drops correspond to higher flow rates (higher Reynolds numbers), wherein the dependency of the friction factor on the Reynolds number diminishes. The reduction of the tube diameter at higher Reynolds number does not severely penalize the flow rate. Therefore lower values of $D$ are required to minimize $R_{tot}$. The low aspect ratio of $L/D$ which minimizes $R_{tot}$, is a result of very high heat transfer coefficients exhibited at the microscale ($h$ is inversely proportional to $D$), as can be seen from Fig. 6. Moreover, this raises an additional physical issue that needs to be carefully examined. Deviation has been found in the Nusselt number [15] and friction factors [16,17] values between short and long fins. However, existing correlations for Nusselt numbers and friction factor in intermediate tubes ($0.5 < L/D < 6$) have been mainly developed for Reynolds numbers corresponding to transition and turbulent flows. Nevertheless, flow across microscale fin arrays typically requires laminar flow models.

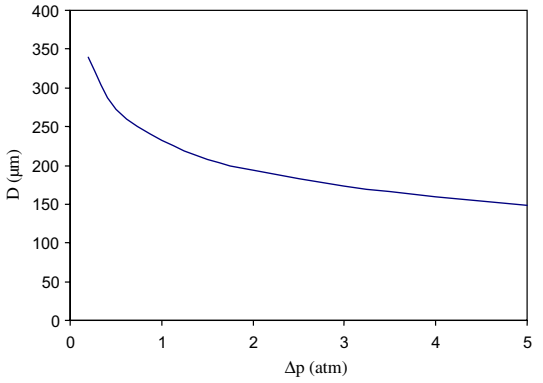


Fig. 5. Optimum $D$ vs. pressure ($L = 400$ μm, $\varepsilon = 0.65$, $w_2/L = 25$).

The minimum $R_{tot}$ value as a function of the pressure drop is shown in Fig. 7. At a pressure drop of two atmospheres, the minimum total thermal resistance ($(R_{tot})_{min}$) is 0.0389 K W$^{-1}$, which corresponds to 7.8 °C maximum wall temperature raise for 200 W cm$^{-2}$ heat dissipation power, and 30.7 °C at 790 W cm$^{-2}$. These values seem to be superior to microchannels flow as demonstrated in Table 1. Although, the microchannel data provided in the table were obtained for optimized conditions, the thermal resistance of the pin fin heat sink is a factor of 1.5–2.5 smaller than for microchannels. For example, Tuckermann and Pease [20] claimed wall temperature rise of 71 °C for heat flux of 790 W cm$^{-2}$ under optimized microchannels configuration for a 30 psi pressure drop. It should be noted that the heat transfer and pressure drop correlations are currently not developed sufficiently to accurately determine the thermal resistance. Nonetheless, the results strongly suggest that pin fin heat sinks have considerable potential as microscale cooling schemes and deserve research consideration analogous to microchannels.

Fig. 8 shows the thermal resistance as a function of porosity for $D = 100$ μm, $L = 400$ μm, $w_2 = 1$ cm, and $\Delta P = 2$ atm. The reduction of $R_{tot}$ with $\varepsilon$ is primarily due to the increasing velocities as flow resistance drops. At porosities larger than ~0.5 the curve is relatively flat. As discussed in the previous section, at very high porosity (0.85 and larger) endwall effects become significant and the model can no longer be considered accurate. In fact, for $\varepsilon = 1$ (no pin fins) the model predicts $R_{tot}$ to be zero, which of course is incorrect. When endwall

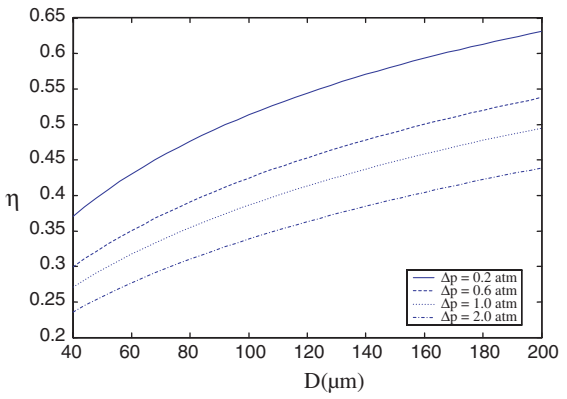


Fig. 6. Fin efficiency vs. $D$ for water ($L = 400$ μm, $\varepsilon = 0.65$, $w_2/L = 25$).

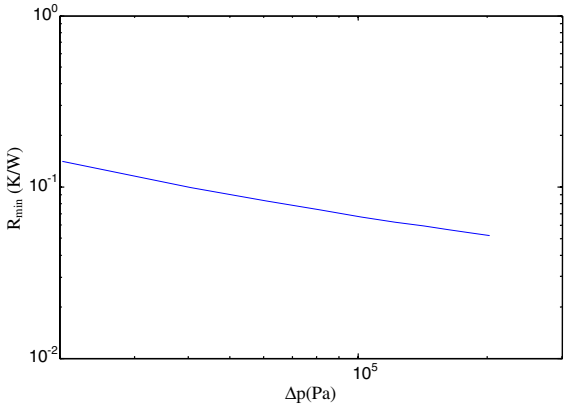


Fig. 7. $R_{min}$ vs. pressure drop profile for water ($L = 400$ μm, $\varepsilon = 0.65$, $w_2/L = 25$).

Table 1
Comparison of thermal performance

| | $\Delta p$ (kPa) | $q''$ (W cm$^{-2}$) | $R$ (K W$^{-1}$) | Cross-section | Hydraulic diameter (μm) | $H$ (μm) | $w_1 \times w_2$ (cm$^2$) | Temperature rise (°C) |
|---|---|---|---|---|---|---|---|---|
| Tuckerman and Pease [20] | 203 | 790 | 0.0900 | Rectangular | 92 | 302 | 1.0 | 71.0 |
| Knight et al. [24] | 207 | 790 | 0.0560 | Circular | 371 | 365 | 1.0 | 44.3 |
| Gillot et al. [29] | 180 | 350 | 0.0920 | Rectangular | 364 | 2000 | 9.0 | 35.0 |
| Murakami and Mikić [27] | 264 | 790 | 0.056 | Circular | 247 | 365 | 1.0 | 44.3 |
| Current study | 203 | 790 | 0.0389 | Rectangular | – | 243 | 1.0 | 30.7 |

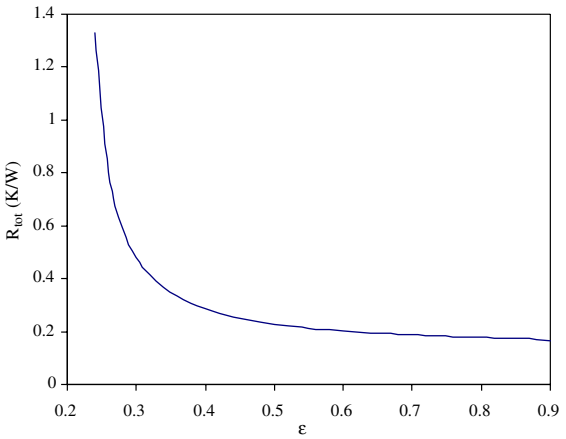


Fig. 8. $R_{tot}$ vs. $\varepsilon$ profile for 2 atm pressure drop.

effects are considered for $\varepsilon = 1$ (a plain high aspect ratio microchannel) the resulting thermal resistance is 2.5 K W$^{-1}$ (much larger than for $0.3 < \varepsilon < 0.85$).

## 4. Experiments

In order to validate the analytical results obtained in the previous section an experimental study is conducted. This section describes the design and fabrication of a micro pin fin heat sink, outlines the experimental procedure and presents the experimental results.

### 4.1. Micro heat sink device fabrication

The micro pin fin heat sink device is micromachined on a polished double-sided *n*-type ⟨100⟩ single crystal silicon wafer employing techniques adapted from IC manufacturing. The microfluidic device used in the present investigation consists of an array of cylindrical pins (transverse and longitudinal pitch ratio of 1.5) embedded inside an 1.8 mm wide, 243 μm deep and 10 mm long channel. The microfluidic device is equipped with pressure ports at the inlet and the exit to obtain accurate static pressure measurements. A schematic representation of the primary steps in the process flow is displayed in Fig. 9.

A 1.5 μm thick high quality thermal oxide is deposited on both sides of the silicon wafer to shield the bare wafer surface during processing. The heater and the via's are formed on the backside of the wafer by CVC sputtering. A 70 A thick layer of Titanium is initially deposited to enhance adhesion characteristics and is followed by sputtering a 1 μm thick layer of Aluminum containing 1% Si. Subsequent photolithography and concomitant wet bench processing creates the heater on the backside of the wafer. A 1 μm thick PECVD (plasma enhanced chemical vapor deposition) oxide is deposited to protect the heater during further processing.

Next, the microchannel and the pins are formed on the top side of the wafer. The wafer is taken through a photolithography step and an oxide removal process (reactive ion etching) to mask certain areas on the wafer, which are not be etched during the DRIE (deep reactive ion etching) process. The wafer is consequently etched in a DRIE process and silicon is removed from places not protected by the photoresist/oxide mask. This creates an array of cylindrical pins entrenched inside a microchannel. In order to minimize ambient heat losses an air gap is formed on the two ends of the side walls (Fig. 10) and 4 mm long inlet and exit plenum are formed on the thin silicon substrate (~150 m). The DRIE process forms

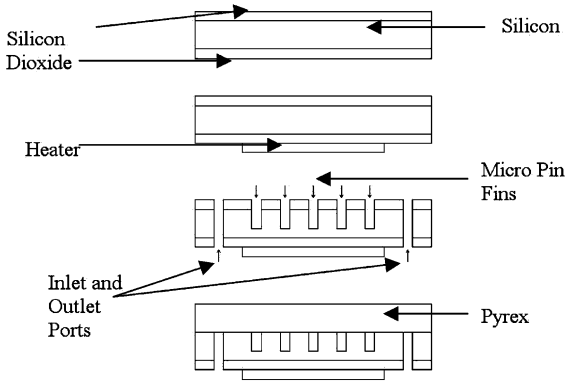


Fig. 9. Process flow of the microfluidic device.

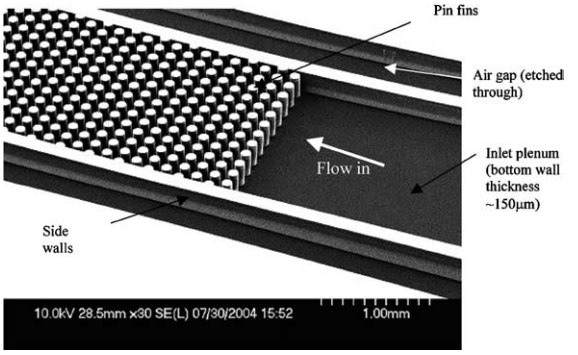


Fig. 10. SEM image of the microfluidic device.

deep vertical trenches on the silicon wafer with a characteristic scalloped sidewall possessing a peak-to-peak roughness of ~0.3 μm. A profilometer is employed to measure and record various dimensions of the device.

The wafer is flipped and the backside is then processed to create an inlet, outlet and pressure port taps for the transducers. A photolithography followed by a BOE (6:1) oxide removal process is carried out to create a pattern mask. The wafer is then etched-through in a DRIE process to create the fluidic ports. Further, electrical contacts/pads are opened up on the backside of the wafer by performing another round of photolithography and RIE processing. Finally, the processed wafer is stripped of any remaining resist or oxide layers and anodically bonded to a 1 mm thick polished Pyrex (glass) wafer to form a sealed device. After successful completion of the bonding process, the processed stack is die-sawed to separate the devices from the parent wafer. An SEM image of the microdevice is shown in Fig. 10 and a two-layer CAD model is presented in Fig. 1 for completeness.

### 4.2. Experimental setup details

The MEMS device is packaged by sandwiching it between two plates as shown in Fig. 11(a). The fluidic seals are forged using miniature "o-rings," while the electrical connections to the heater are achieved from beneath through spring-loaded pins. A microgear pump is used to propel the liquid from a reservoir through the MEMS device at various flow rates (Fig. 11(b)). A Welch vacuum pump is employed to remove air in the system prior to any liquid circulation. Flow data is measured via pressure transducers and an Omega flow meter and stored/analyzed using an IBM PC. The pin fin heat sink is continuously scrutinized using a microscope and a CCD camera combination unit.

### 4.3. Experimental procedure

At first, the temperature dependency of the electrical resistance of the heater is obtained using a temperature controlled oven, and a calibration curve is attained. Next, the reservoir pressure is fixed, and a constant flow rate is realized by operating the micropump. Experimental data from the flow meter and the pressure transducers is collected once steady flow conditions have been accomplished. A Lab View® interface is employed for data collection and concomitant analysis. All experiments are performed with de-ionized water as the working fluid. Thereafter, a voltage is applied across the device, and current and voltage information are recorded once stable conditions have been reached. The voltage is increased in increments of 0.5 V up to maximum of 10 V, and electrical data is continuously acquired. This data is used to determine the resistance of the device at those conditions. Further data reduction leads to the determination of temperature of the device at different power inputs. The uncertainties of the measured values, given in Table 2, are derived from the manufacturer's specification sheets, while the uncertainties of the derived parameters are obtained using the method developed by Kline and McClintock [30].

### 4.4. Data reduction

The raw data (i.e., voltage, current, flow rates, pressures) measured in the experiments are further processed to obtain certain quantities. The electrical power can be expressed in terms of current and voltage recorded earlier as

$$P = E \cdot I \tag{23}$$

From the voltage and current data, the experimental electrical resistance can be determined as follows:

$$R_{\text{exp}} = E/I \tag{24}$$

Once experimental electrical resistances have been determined, they are converted to average temperatures values using the previously obtained calibration curve. With $P$ and $T_{\text{av}}$ known, the dimensional thermal resistance $R_{\text{tot}}$ is easily calculated as

$$R_{\text{tot}} = \frac{2(T_{\text{av}} - T_{\text{amb}})}{P} = \frac{2\Delta T_{\text{av}}}{P} \tag{25}$$

The factor 2 in Eq. (25) accounts for the discrepancy between the measured wall temperature (the average) and the temperature used to define the thermal resistance (at the exit). A mean absolute error (MAE) of the experimental results with theoretical values is given by:

$$\text{MAE} = \frac{1}{M}\sum_{i=1}^{i=M} \frac{|X_{\text{tot,exp}} - X_{\text{tot,theoretical}}|}{X_{\text{tot,exp}}} \times 100\% \tag{26}$$

One-dimensional fin analysis on the inlet and outlet plenum is performed to estimate heat losses from the micro pin fin sink. The analysis yields a heat loss which is 6.2%

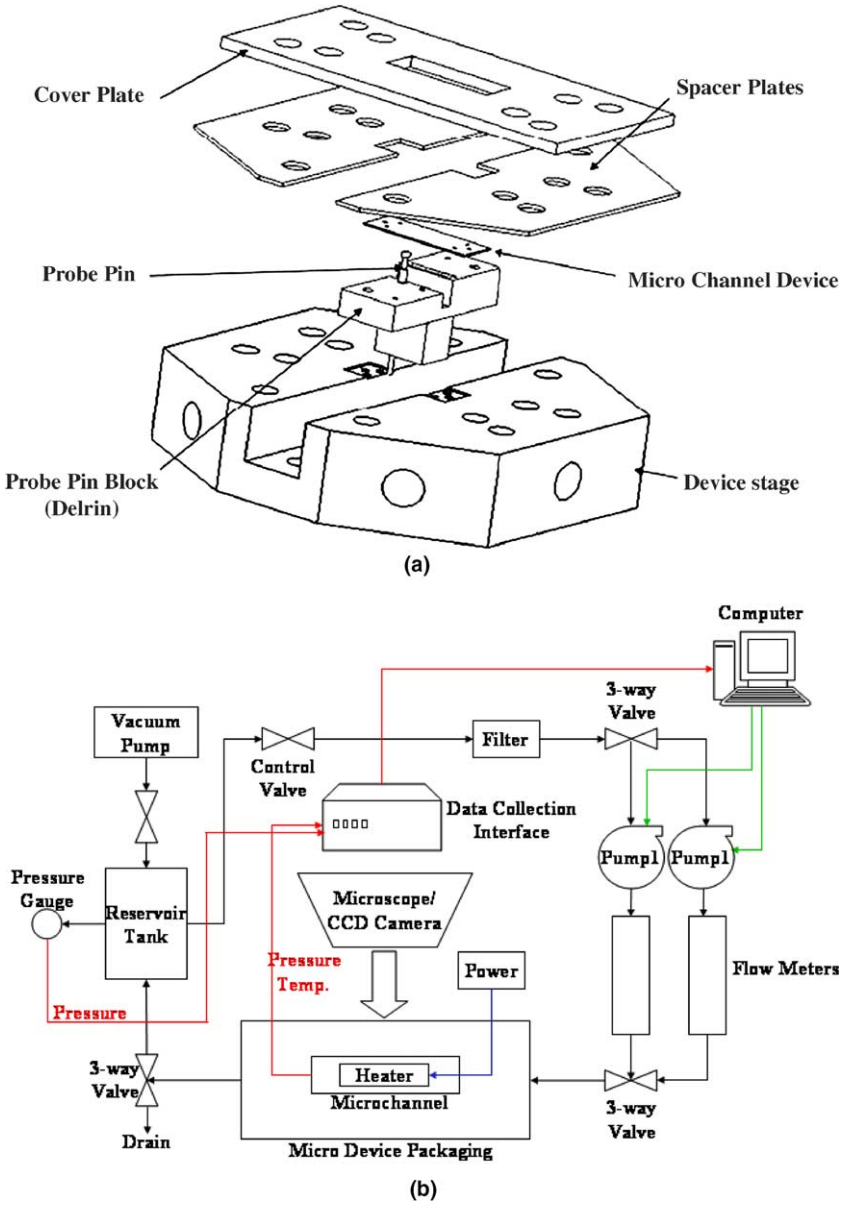


Fig. 11. (a) Device package and (b) experimental setup.

Table 2
Uncertainties in variables used in uncertainty analysis

| Uncertainty | Error |
|---|---|
| Flow rate, $Q$ (for each reading) | ±1.0% |
| Voltage supplied by power source, $V$ | ±0.5% |
| Current supplied by power source, $I$ | ±0.5% |
| Ambient temperature, $T_{amb}$ | ±0.1 °C |
| Electrical power, $P$ | ±0.7% |
| Electrical resistance, $R$ | ±0.7% |
| Average temperature, $T_{av}$ | ±2.0 °C |
| $\overline{R}_{tot}$ | ±3.1% |
| $f$ | 7.2% |

of the electrical power supplied to the heater. Heat loss from the bottom surface is estimated by assuming one-dimensional conduction through a 2 mm air gap (gap between the chip bottom and the top pin block), while thermal losses comprising of conduction through the pyrex substrate and natural convection is used to estimate heat loss from the top surface. Maximum heat losses from the top and bottom surfaces yield ~0.02 W and ~0.01 W, which is considerably smaller than heat losses from the inlet and outlet plenum. Thus, heat losses from the top and bottom surfaces are neglected.

### 4.5. Experimental results

#### 4.5.1. Heat transfer

Fig. 12 shows the experimental average wall temperature, $\Delta T_{av}$, as a function of heat flux, $q''$, for flow rate of 3.2 ml/min (corresponding to frontal velocity of 0.317 m $s^{-1}$) together with the analytical expression obtained with Eq. (14). As can be seen the experimental results compare very favorably with the analytical expression, with a mean absolute error of 5.7%. Theoretical total thermal resistance and the experimental results are shown in Fig. 13, which again display good agreement. The MAE in this case is 5.2% and the ratios between experimental and theoretical values fall between 0.8 and 1.2 as shown in Fig. 14. It should be noted that wall temperature rise is primarily due to the increase in the water temperature, and the contribution of the convective term is relatively small (15–20% of the total thermal resistance). A relatively large deviation of Eq. (13) from the actual Nusselt number would not necessarily result in a large deviation between the experimental results and Eq. (14). Since the convective heat transfer is very effective, surface temperatures are very comparable to the fluid temperatures. Small measurements uncertainties of both temperatures will propagate to large experimental uncertainties in the heat transfer coefficient. In order to obtain accurate Nusselt number correlations experimentally, it is necessary to either perform experiments at very high heat fluxes (increases wall-fluid temperature drop) or use fluids having a low thermal conductivity (reduces heat transfer coefficient while maintaining the same Reynolds and *Pr* number).

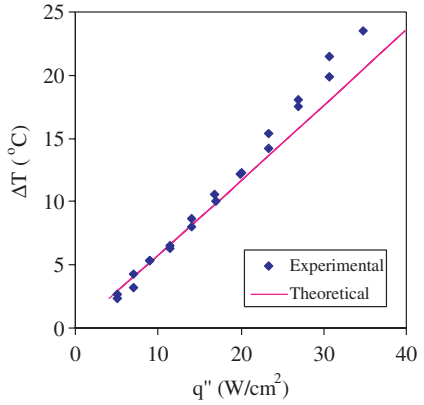


Fig. 12. $\Delta T_{av}$ vs. $q''$ ($Q$ = 3.2 ml/min, $\Delta p$ = 14.7 kPa, $\varepsilon$ = 0.65, and $w_2/L$ = 41).

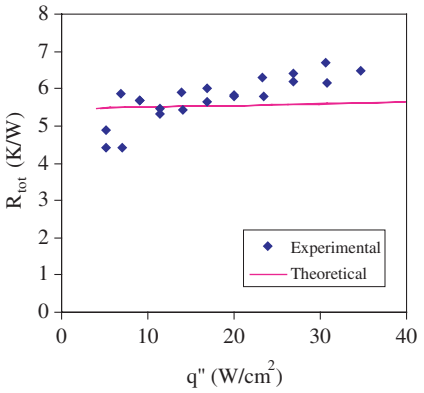


Fig. 13. $R_{tot}$ vs. $q''$ ($Q$ = 3.2 ml/min, $\Delta p$ = 14.7 kPa, $\varepsilon$ = 0.65, and $w_2/L$ = 41).

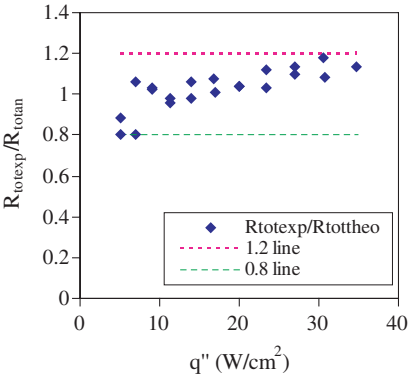


Fig. 14. $R_{tot,exp}/R_{tot,theoretical}$ vs. $q''$ ($Q$ = 3.2 ml/min, $\Delta p$ = 14.7 kPa, $\varepsilon$ = 0.65, and $w_2/L$ = 41).

#### 4.5.2. Pressure drop

Adiabatic tests were performed over a wide range of flow rates and pressure drops. Fig. 15 shows the corresponding friction factor as a function of Reynolds number along with several laminar flow correlations developed using conventional scale apparatus [12,16,28,31] and data collected from microscale pin fin geometries [17]. The MAE's between the experimental data, the various correlations and published data are

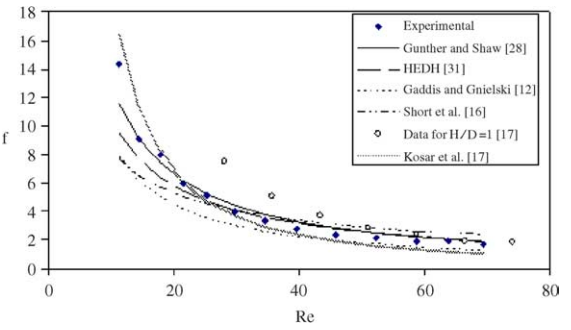


Fig. 15. Friction factor as a function of Reynolds number.

Table 3
Mean average error of friction factor between experimental data and available correlations

| | Gaddis and Gnielski [12] | Gunther and Shaw [28] | Short et al. [16] | HEDH [31] | Koşar et al. [17] |
|---|---|---|---|---|---|
| MAE (%) | 27.7 | 11.1 | 24.9 | 14.3 | 17.9 |

presented in Table 3. It is clear from Fig. 15 that the data correlates fairly well with an MAE range between 11.1 and 27.7 (depending on the correlation). A distinct difference between the data obtain by Koşar et al. [17] for $L/D = 1$ and the current device $L/D = 2.43$ is evident (the two devices are identical excluding $L/D$ values). As discussed in [17], endwall effects for friction factor across laminar flow over microscale pin fins are important for fin pins height-to-diameter smaller than some value between 1 and 2 (the exact value was not specified). Since for the current device $L/D$ ratio is larger than 2, endwall effects diminishes and the long tube correlations fit the experimental data. It should be noted that in many circumstances optimization can provide $L/D$ values in the 1–2 range. For this range, correlations that account for endwall effects in laminar flow (such as [16,17]) should be used.

## 5. Conclusions

In this study, a comprehensive heat transfer analysis over a bank of micro pin fins has been conducted analytically and the concomitant results have been experimentally validated. A simplified expression for the total thermal resistance has been derived and discussed. The main conclusions drawn from this investigation are presented below:

- Very high heat fluxes can be dissipated at low wall temperature rise using a microscale pin fin heat sink. The thermo-hydraulic performance of flow across a microscale cylindrical pin fin array is superior to plain microchannel based cooling. The heat transfer and pressure drop correlations are currently not sufficiently developed, but the results strongly suggest that pin fin heat sinks deserve adequate research attention. Furthermore, pin fin configurations provide considerably more design flexibility in the geometrical selection of the pin shapes and their spacing.
- Forced convection over shrouded micro pin fin heat sinks is a very effective heat transfer mode. In many cases, the primary cause for the rise in wall temperature is the increase of the fluid temperature as it flows through the heat sink.
- To suppress the convective thermal resistance at high Reynolds number dense pin fin configurations are preferable, while for low Reynolds numbers more sparse arrangements are advisable.
- Very low tube diameters (below ~50 μm) should be avoided. The thermal resistance is less sensitive to changes in the tube diameter at larger diameters.
- Heat transfer coefficients for microscale pins are very large and result in decreasing fin efficiencies. To increase efficiencies, pins should be relatively short. However, correlations for low Reynolds number (applicable to microscale systems) heat transfer coefficients for intermediate pins length are very scarce.

## References

[1] W. Qu, G. Mala, L. Dongqing, Pressure-driven water flows in trapezoidal silicon microchannels, Int. J. Heat Mass Transfer 43 (3) (2000) 353–364.
[2] S.M. Ghiaasiaan, T.S. Laker, Turbulent forced convection in microtubes, Int. J. Heat Mass Transfer 44 (14) (2001) 2777–2782.
[3] X.F. Peng, G.P. Peterson, Convective heat transfer and flow friction for water flow in microchannel structure, Int. J. Heat Mass Transfer 39 (12) (1996) 2599–2608.
[4] S.G. Kandlikar, W.J. Grande, Evaluation of single phase flow in microchannels for high flux chip cooling—thermohydraulic performance enhancement and fabrication technology, in: Presented at the Second International Conference on Microchannels and Minichannels, ASME, New York, 2004, pp. 67–76.
[5] L. Zhang, J. Koo, L. Jiang, M. Asheghi, K.E. Goodson, J.G. Santiago, Measurements and modeling of two-phase flow in microchannels with nearly constant heat flux boundary conditions, J. Microelectromech. Syst. 11 (1) (2002) 12–19.
[6] L. Jiang, M. Wong, Y. Zohar, Forced convection boiling in microchannel heat sink, J. Microelectromech. Syst. 10 (1) (2001) 80–87.
[7] S.G. Kandlikar, Fundamental issues related to flow boiling in minichannels and microchannels, Exp. Therm. Fluid Sci. 26 (2002) 389–407.
[8] S.G. Kandlikar, Two-phase flow patterns, pressure drop, and heat transfer during Boiling in minichannels flow passages of compact evaporators, Heat Transfer Eng. 23 (1) (2002) 5–23.
[9] W. Qu, I. Mudawar, Flow boiling heat transfer in two-phase micro-channel heat sink—I. Experimental investigation and assessment of correlation methods, Int. J. Heat Mass Transfer 46 (15) (2003) 2755–2771.
[10] A.A. Zukauskas, Heat transfer from tubes in cross flowAdvances in Heat Transfer, vol. 8, Academic Press, New York, 1972, pp. 93–160.
[11] V.T. Morgan, The overall convective heat transfer from smooth circular cylinders, in: T.F. Irvine, Jr., J.P. Hartnett

(Eds.), Advances in Heat Transfer, vol. 11, Academic Press, New York, pp. 199–264.
[12] E.S. Gaddis, V. Gnielski, Pressure drop in horizontal cross flow across tube bundles, Int. Chem. Eng. 25 (1) (1985) 1–15.
[13] K.A. Moores, Y.K. Joshi, Effect of tip clearance on the thermal and hydrodynamic performance of a shrouded pin fin array, J. Heat Transfer 125 (6) (2003) 999–1006.
[14] R.L. Webb, Air-side heat transfer in finned tube heat exchangers, Heat Transfer Eng. 1 (1980) 33–49.
[15] J. Armstrong, D. Winstanley, A review of staggered array pin fin heat transfer for turbine cooling applications, J. Turbomach. 110 (1988) 94–103.
[16] B.E. Short Jr., P.E. Raad, D.C. Price, Performance of pin fin cast aluminum coldwalls. Part 1: friction factor correlations, J. Thermophys. Heat Transfer 16 (3) (2002) 389–396.
[17] A. Koşar, C. Mishra, Y. Peles, Laminar flow across a bank of low aspect ratio micro pin fins, J. Fluids Eng. 127 (3) (2005).
[18] C. Marques, K.W. Kelly, Fabrication and performance of a pin fin micro heat exchanger, J. Heat Transfer 126 (3) (2004) 434–444.
[19] F.P. Incropera, D.P. DeWitt, Introduction to Heat Transfer, fourth ed., Wiley, New York, 2002, pp. 396.
[20] D.B. Tuckerman, R.F.W. Pease, High-performance heat sinking for VLSI, IEEE Electron Dev. Lett. EDL 2 (5) (1981) 126–129.
[21] F.P. Incropera, Liquid Cooling of Electronic Devices by Single-phase Convection, Wiley, New York, 1999.
[22] S. Sasaki, T. Kishimoto, Optical structure for microgrooved cooling fin for high-power LSI devices, Electron Lett. (22) (1986) 1332–1334.
[23] R.J. Phillips, L.R. Glicksman, R. Larson, Forces-convection, liquid-cooled, microchannel heat sinks for high-powered-density microelectronics, in: Cooling Technology for Electronic Equipment, Hemisphere, New York, 1998, pp. 295–316.
[24] R.W. Knight, D.J. Hall, J.S. Goodling, R.C. Jaeger, Heat sink optimization with application to microchannel, IEEE Trans. Comp. Hybrids Manufact. Technol. (15) (1992) 832–842.
[25] S. Lee, Optimum design and selection of heat sinks, IEEE Trans. Comp. Packag. Manufact. Technol. A (18) (1995) 812–817.
[26] M.B. Kleiner, S.A. Kühn, K. Harberger, High performance forced air cooling scheme employing microchannel heat exchangers, IEEE Trans. Comp. Packag. Manufact. Technol. A (18) (1995) 795–804.
[27] Y. Murakami, B.B. Mikić, Parametric optimization of multichanneled heat sinks for VLSI chip cooling, IEEE Trans. Comp. Packag. Technol. 24 (1) (2001) 2–9.
[28] A.Y. Gunther, W.A. Shaw, A general correlation of friction factors for various types of surfaces in cross flow, Trans. Am. Soc. Mech. Engr. 67 (1945) 643–660.
[29] C. Gilliot, C. Schaeffer, A. Bricard, Integrated micro heat sink for power multichip module, IEEE Trans. Indust. Appl. 36 (1) (2000) 217–221.
[30] S. Kline, F.A. McClintock, Describing uncertainties in single-sample experiments, Mech. Eng. 75 (1) (1953) 3–8.
[31] J. Taborek, Shell-and-tube Heat Exchangers: Single Phase Flow, Handbook of Heat Exchanger Design, Hemisphere, New York, 1983 (Chapter 3.3).